Multiple Fano resonances in single-layer nonconcentric core-shell nanostructures

Zhang, Jingjing; Zayats, Anatoly

Published in:
Optics Express

Link to article, DOI:
10.1364/OE.21.008426

Publication date:
2013

Document Version
Publisher's PDF, also known as Version of record

Multiple Fano resonances in single-layer nonconcentric core-shell nanostructures

Jingjing Zhang,[1,2,*] and Anatoly Zayats[1]

[1]*Department of Physics, King's College London, Strand, London WC2R 2LS, UK*
[2]*Technical University of Denmark, Department of Photonics Engineering-DTU, Denmark*
[*]*jingjing.zhang@kcl.ac.uk*

Abstract: Multiple plasmonic Fano resonances are generally considered to require complex nanostructures, such as multilayer structure, to provide several dark modes that can couple with the bright mode. In this paper, we show the existence of multiple Fano resonances in single layer core-shell nanostructures where the multiple dark modes appear due to the geometrical symmetry breaking induced by axial offset of the core. Both dielectric-core-metal-shell (DCMS) and metal-core-dielectric-shell (MCDS) configurations have been studied. Compared to the MCDS structure, the DCMS configuration provides higher modulation depth. Analytical studies based on transformation optics and numerical simulations have been performed to investigate the role of geometrical and material parameters on the optical properties of the proposed nanostructures. Refractive index sensing with higher-order Fano resonances has also been described, providing opportunity for multiwavelength sensing with high figure of merit.

OCIS codes: (260.5740) Resonance; (240.6680) Surface plasmons; (160.4760) Optical properties.

References and links

1. A. V. Zayats and I. I. Smolyaninov, "Near-field photonics: surface plasmon polaritons and localised surface plasmons," J. Opt. A, Pure Appl. Opt. **5**(4), S16–S50 (2003).
2. J. B. Pendry, A. Aubry, D. R. Smith, and S. A. Maier, "Transformation optics and subwavelength control of light," Science **337**(6094), 549–552 (2012).
3. A. Aubry, D. Y. Lei, A. I. Fernández-Domínguez, Y. Sonnefraud, S. A. Maier, and J. B. Pendry, "Plasmonic light-harvesting devices over the whole visible spectrum," Nano Lett. **10**(7), 2574–2579 (2010).
4. Y. Luo, J. B. Pendry, and A. Aubry, "Surface plasmons and singularities," Nano Lett. **10**(10), 4186–4191 (2010).
5. A. I. Fernández-Domínguez, S. A. Maier, and J. B. Pendry, "Collection and concentration of light by touching spheres: a transformation optics approach," Phys. Rev. Lett. **105**(26), 266807 (2010).
6. Y. Luo, D. Y. Lei, S. A. Maier, and J. B. Pendry, "Broadband light harvesting nanostructures robust to edge bluntness," Phys. Rev. Lett. **108**(2), 023901 (2012).
7. F. Hao, Y. Sonnefraud, P. V. Dorpe, S. A. Maier, N. J. Halas, and P. Nordlander "Symmetry breaking in plasmonic nanocavities: subradiant LSPR sensing and a tunable Fano resonance," Nano Lett. **8**(11), 3983–3988 (2008).
8. A. I. Kuznetsov, A. B. Evlyukhin, M. R. Gonçalves, C. Reinhardt, A. Koroleva, M. L. Arnedillo, R. Kiyan, O. Marti, and B. N. Chichkov, "Laser fabrication of large-scale nanoparticle arrays for sensing applications," ACS Nano **5**(6), 4843–4849 (2011).
9. M. A. Noginov, G. Zhu, A. M. Belgrave, R. Bakker, V. M. Shalaev, E. E. Narimanov, S. Stout, E. Herz, T. Suteewong, and U. Wiesner, "Demonstration of a spaser-based nanolaser," Nature **460**(7259), 1110–1112 (2009).
10. W. Zhang, A. O. Govorov, and G. W. Bryant, "Semiconductor-metal nanoparticle molecules: Hybrid excitons and the nonlinear Fano effect," Phys. Rev. Lett. **97**(14), 146804 (2006).
11. A. E. Miroshnichenko, S. F. Mingaleev, S. Flach, and Y. S. Kivshar, "Nonlinear Fano resonance and bistable wave transmission," Phys. Rev. E Stat. Nonlin. Soft Matter Phys. **71**(3 3 Pt 2B), 036626 (2005).
12. U. Fano, "The Theory of Anomalous Diffraction Gratings and of quasi-stationary waves on metallic surfaces (Sommerfeld's Waves)," J. Opt. Soc. Am. **31**(3), 213–222 (1941).
13. A. E. Miroshnichenko, S. Flach, and Y. S. Kivshar, "Fano resonances in nanoscale structures," Rev. Mod. Phys. **82**(3), 2257–2298 (2010).
14. B. Luk'yanchuk, N. I. Zheludev, S. A. Maier, N. J. Halas, P. Nordlander, H. Giessen, and C. T. Chong, "The Fano resonance in plasmonic nanostructures and metamaterials," Nat. Mater. **9**(9), 707–715 (2010).

#183368 - $15.00 USD Received 14 Jan 2013; revised 4 Mar 2013; accepted 4 Mar 2013; published 29 Mar 2013

15. F. Hao, P. Nordlander, Y. Sonnefraud, P. V. Dorpe, and S. A. Maier, "Tunability of subradiant dipolar and Fano-type plasmon resonances in metallic ring/disk cavities: Implications for nanoscale optical sensing," ACS Nano **3**(3), 643–652 (2009).
16. Y. Sonnefraud, N. Verellen, H. Sobhani, G. A. E. Vandenbosch, V. V. Moshchalkov, P. Van Dorpe, P. Nordlander, and S. A. Maier, "Experimental realization of subradiant, superradiant, and Fano resonances in ring/disk plasmonic nanocavities," ACS Nano **4**(3), 1664–1670 (2010).
17. Y. H. Fu, J. B. Zhang, Y. F. Yu, and B. Luk'yanchuk, "Generating and manipulating higher order Fano resonances in dual-disk ring plasmonic nanostructures," ACS Nano **6**(6), 5130–5137 (2012).
18. S. Zhang, D. A. Genov, Y. Wang, M. Liu, and X. Zhang, "Plasmon-induced transparency in metamaterials," Phys. Rev. Lett. **101**(4), 047401 (2008).
19. N. Liu, L. Langguth, T. Weiss, J. Kästel, M. Fleischhauer, T. Pfau, and H. Giessen, "Plasmonic analogue of electromagnetically induced transparency at the Drude damping limit," Nat. Mater. **8**(9), 758–762 (2009).
20. J. Zhang, S. Xiao, C. Jeppesen, A. Kristensen, and N. A. Mortensen, "Electromagnetically induced transparency in metamaterials at near-infrared frequency," Opt. Express **18**(16), 17187–17192 (2010).
21. A. Artar, A. A. Yanik, and H. Altug, "Multispectral plasmon induced transparency in coupled meta-atoms," Nano Lett. **11**(4), 1685–1689 (2011).
22. Z. Y. Fang, J. Y. Cai, Z. B. Yan, P. Nordlander, N. J. Halas, and X. Zhu, "Removing a wedge from a metallic nanodisk reveals a Fano resonance," Nano Lett. **11**(10), 4475–4479 (2011).
23. F. López-Tejeiral, R. Paniagua-Domínguez, R. Rodríguez-Oliveros, and J. A. Sánchez-Gil, "Fano-like interference of plasmon resonances at a single rod-shaped nanoantenna," New J. Phys. **14**(2), 023035 (2012).
24. J. B. Lassiter, H. Sobhani, J. A. Fan, J. Kundu, F. Capasso, P. Nordlander, and N. J. Halas, "Fano resonances in plasmonic nanoclusters: Geometrical and chemical tunability," Nano Lett. **10**(8), 3184–3189 (2010).
25. S. D. Liu, Z. Yang, R. P. Liu, and X. Y. Li, "Multiple Fano resonances in plasmonic heptamer clusters composed of split nanorings," ACS Nano **6**(7), 6260–6271 (2012).
26. G. Bachelier, I. Russier-Antoine, E. Benichou, C. Jonin, N. Del Fatti, F. Vallée, and P. F. Brevet, "Fano profiles induced by near-field coupling in heterogeneous dimers of gold and silver nanoparticles," Phys. Rev. Lett. **101**(19), 197401 (2008).
27. K. C. Woo, L. Shao, H. J. Chen, Y. Liang, J. F. Wang, and H. Q. Lin, "Universal scaling and Fano resonance in the plasmon coupling between gold nanorods," ACS Nano **5**(7), 5976–5986 (2011).
28. H. J. Chen, L. Shao, Y. C. Man, C. M. Zhao, J. F. Wang, and B. C. Yang, "Fano resonance in (gold core)-(dielectric shell) nanostructures without symmetry breaking," Small **8**(10), 1503–1509 (2012).
29. S. Mukherjee, H. Sobhani, J. B. Lassiter, R. Bardhan, P. Nordlander, and N. J. Halas, "Fanoshells: nanoparticles with built-in Fano resonances," Nano Lett. **10**(7), 2694–2701 (2010).
30. D. J. Wu, S. M. Jiang, and X. J. Liu, "Tunable Fano resonances in three-layered bimetallic Au and Ag nanoshell," J. Phys. Chem. C **115**(48), 23797–23801 (2011).
31. C. Argyropoulos, P. Y. Chen, F. Monticone, G. D'Aguanno, and A. Alù, "Nonlinear plasmonic cloaks to realize giant all-optical scattering switching," Phys. Rev. Lett. **108**(26), 263905 (2012).
32. F. Monticone, C. Argyropoulos, and A. Alu, "Multi-layered plasmonic covers for comb-like scattering response and optical tagging," Arxiv:1210.4802.
33. A. L. Aden and M. Kerker, "Scattering of electromagnetic waves from two concentric spheres," J. Appl. Phys. **22**(10), 1242–1246 (1951).
34. R. D. Averitt, S. L. Westcott, and N. J. Halas, "Linear optical properties of gold nanoshells," J. Opt. Soc. Am. B **16**(10), 1824–1832 (1999).
35. F. Tam, C. Moran, and N. J. Halas, "Geometrical parameters controlling sensitivity of nanoshell plasmon resonances to changes in dielectric environment," J. Phys. Chem. B **108**(45), 17290–17294 (2004).
36. R. Bardhan, N. K. Grady, T. Ali, and N. J. Halas, "Metallic nanoshells with semiconductor cores: Optical characteristics modified by core medium properties," ACS Nano **4**(10), 6169–6179 (2010).
37. H. Wang, Y. P. Wu, B. Lassiter, C. L. Nehl, J. H. Hafner, P. Nordlander, and N. J. Halas, "Symmetry breaking in individual plasmonic nanoparticles," Proc. Natl. Acad. Sci. U.S.A. **103**(29), 10856–10860 (2006).
38. J. B. Lassiter, M. W. Knight, N. A. Mirin, and N. J. Halas, "Reshaping the plasmonic properties of an individual nanoparticle," Nano Lett. **9**(12), 4326–4332 (2009).
39. Y. Lu, G. L. Liu, J. Kim, Y. X. Mejia, and L. P. Lee, "Nanophotonic crescent moon structures with sharp edge for ultrasensitive biomolecular detection by local electromagnetic field enhancement effect," Nano Lett. **5**(1), 119–124 (2005).
40. E. Prodan, C. Radloff, N. J. Halas, and P. Nordlander, "A hybridization model for the plasmon response of complex nanostructures," Science **302**(5644), 419–422 (2003).
41. A. Christ, S. G. Tikhodeev, N. A. Gippius, J. Kuhl, and H. Giessen, "Waveguide-plasmon polaritons: strong coupling of photonic and electronic resonances in a metallic photonic crystal slab," Phys. Rev. Lett. **91**(18), 183901 (2003).
42. M. W. Klein, T. Tritschler, M. Wegener, and S. Linden, "Lineshape of harmonic generation by metallic nanoparticles and metallic photonic crystal slabs," Phys. Rev. B **72**(11), 115113 (2005).
43. V. Giannini, Y. Francescato, H. Amrania, C. C. Phillips, and S. A. Maier, "Fano resonances in nanoscale plasmonic systems: A parameter-free modeling approach," Nano Lett. **11**(7), 2835–2840 (2011).
44. F. Borghese, P. Denti, R. Saija, and O. I. Sindoni, "Optical properties of spheres containing a spherical eccentric inclustion," J. Opt. Soc. Am. A **9**(8), 1327–1335 (1992).
45. N. C. Skaropoulos, M. P. Ioannidou, and D. P. Chrissoulidis, "Indirect mode-matching solution to scattering from a dielectric sphere with an eccentric inclusion," J. Opt. Soc. Am. A **11**(6), 1859–1866 (1994).

#183368 - $15.00 USD Received 14 Jan 2013; revised 4 Mar 2013; accepted 4 Mar 2013; published 29 Mar 2013

46. K. A. Fuller, "Scattering and absorption cross sections of compounded spheres. III. Spheres containing arbitrarily located spherical inhomogeneities," J. Opt. Soc. Am. A **12**(5), 893–904 (1995).
47. A. Aubry, D. Y. Lei, S. A. Maier, and J. B. Pendry, "Interaction between plasmonic nanoparticles revisited with transformation optics," Phys. Rev. Lett. **105**(23), 233901 (2010).
48. A. Aubry, D. Y. Lei, S. A. Maier, and J. B. Pendry, "Conformal transformation applied to plasmonics beyond the quasistatic limit," Phys. Rev. B **82**(20), 205109 (2010).
49. J. A. Kong, *Electromagnetic Wave Theory, II* (Wiley, 1990).
50. A. I. Fernández-Domínguez, Y. Luo, A. Wiener, J. B. Pendry, and S. A. Maier, "Theory of three-dimensional nanocrescent light harvesters," Nano Lett. **12**(11), 5946–5953 (2012).

1. Introduction

Localized surface plasmons (LSPs) sustained by plasmonic nanostructures depend strongly on the geometry and size of the structures and the surrounding materials [1]. This property enables the engineering of the spectral characteristics of LSP resonances. With proper design of the nanoparticles it is possible to achieve broadband response for light harvesting [2–6] or extremely narrow bandwidth response for applications such as biosensing [7,8], lasing [9] and photoswitching [10, 11]. Recently, considerable attention has been paid to plasmonic Fano resonances, which is a classical analogue of the Fano resonances of a quantum particle scattered by a potential with quasidiscrete levels [12]. The plasmonic Fano resonance has extremely narrow linewidth due to the coupling between the broad bright resonance mode and the narrow dark modes supported by plasmonic nanostructures [13, 14], and is intrinsically extremely sensitive to changes in geometry or local environment. Various structures have been proposed to achieve Fano resonances, such as ring/disk nanocavities [7, 15–17], plasmonic metamaterials [18–21], modified nanodisks [22], single rod-shaped nanoantenna [23], nano-clusters [24, 25], heterodimer structures [26, 27], and nano-shells [28–32]. Among those numerous designs, considerable attempts have been made to achieve multiple Fano-resonances [17, 21, 29, 30, 32], that enable the applications to be explored simultaneously at different frequencies. In all these approaches, multiple components (or multi-layers) are involved in the elementary plasmonic nanoparticle to provide several dark modes that couple with the bright mode. Up to date, multiple plasmonic Fano resonances have rarely been observed in simple individual nanostructures like single-layer nanoshells.

In this article, we will show that multiple Fano resonances can be realized by nanostructures without introducing extra elements. Our design is based on the core-shell nano-structure [33–36], in dielectric-core-metal-shell (DCMS) and metal-core-dielectric-shell (MCDS) configurations. With analytical method based on transformation optics and numerical simulations, we show that for both configurations, introducing the symmetry breaking by the core displacement induces the appearance of higher-order multiple Fano resonances. Moreover, increasing the offset of the core results in a red shift of the resonance modes in the DCMS configuration and a blue shift in the MCDS geometry. Compared to the MCDS structure, the DCMS configuration is a better candidate for achieving and exploiting multiple Fano resonances since it provides higher modulation depth of the spectral response. We also show that appropriate choice of the inner core material allows the tailoring of the Fano resonance modes within the broad optical spectral range. Figure of merit for multiwavelength refractive index sensing with higher-order Fano resonances has been estimated. Since experimental realization of nanoshells with symmetry breaking has already been reported [37–39], we expect that the nonconcentric core-shell nanowires designed in this work can be implemented in active optical devices and applied in multifrequency molecular sensing and SERS.

2. Theoretical analysis

Our staring point is a nanoshell structure consisting of a cylindrical dielectric core surrounded by metallic shell (Fig. 1). According to the plasmonic hybridization model [40], such symmetric core-shell structure can support an anti-bonding mode with a weak intensity, which can strongly couple to the broadband dipole mode of the metallic shell. To achieve Fano resonances at multiple frequencies, multiple dark modes are usually required, which can

#183368 - $15.00 USD Received 14 Jan 2013; revised 4 Mar 2013; accepted 4 Mar 2013; published 29 Mar 2013

simultaneously interfere with a broadband bright mode. One strategy is to use multi-layer core-shell structure, where a number of dark modes are introduced by the hybridization between different layers [30, 32]. However, this multi-layer configuration often increases the difficulty in fabrication. Here, we propose to use the non-concentric nano-shells, where higher-order modes are the result of the geometrical symmetry breaking.

The two structures under consideration are shown in Fig. 1(a). The polarization of the illumination is also depicted, where the magnetic field is along the axis of the core. In the following, we always use silver as a metal core or a metal shell with the dielectric constant described by the Drude model $\varepsilon_m = \varepsilon_\infty - \omega_p^2 / \omega(\omega + i\gamma)$, with $\varepsilon_\infty = 3.7$, ω_p=2180 *THz*, γ=4.35 *THz* .

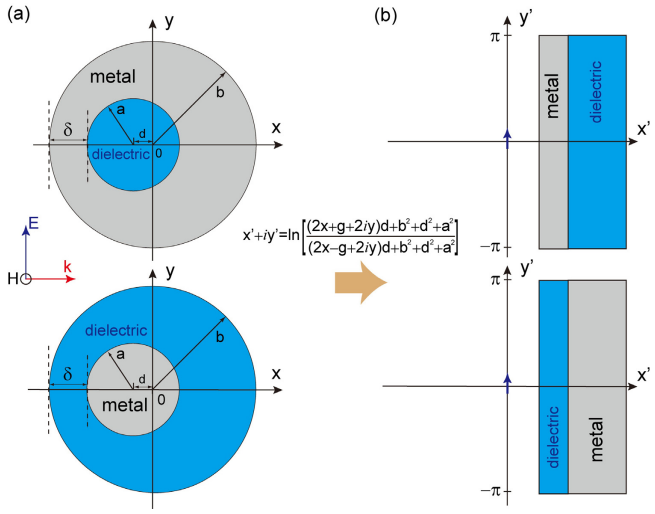

Fig. 1. Schematics of two non-concentric core-shell configurations, i.e. a metal coated dielectric nanowire and a dielectric coated metallic nanowire, illuminated by a plane wave. Here *d* denotes the distance between the centres of the core and the coating; δ denotes the minimum thickness of the coating; the radii of the core and the shell are *a* and *b*, respectively. (b) The transformed geometry of the core-shell structures is represented by an air-metal-dielectric (or air-dielectric-metal) three-layer system. The incident plane wave is mapped into a dipole source located at the origin. Periodic boundary condition is applied along the *y* direction.

Usually, theoretical study of plasmonic Fano resonances requires fitting them with a Fano profile by means of a scattering matrix method [41] or a classical phenomenological model consisting of coupled resonators [42]. Although these methods can give qualitative agreements with experiments, they may not provide enough physical insight and require some fitting parameters (such as the linewidths of bright and dark modes, and the coupling strength between them) to obtain the exact spectrum of the Fano resonance. A more precise approach based on calculations of the probability of mixed states was proposed by Giannini *et al*, which allows for proper understanding of the plasmonic modes in Fano interference [43]. Here, we use the theory of transformation optics (TO) [2–6] to investigate the asymmetric core-shell structures depicted in Fig. 1(a). This approach allows for full wave study of the plasmonic responses of the structures, and offers a route to predict the Fano spectrum without any fitting parameters.

The symmetric core-shell structure (i.e., d = 0) can be investigated with classical Mie scattering theory. When the inner core radius is much smaller than the outer radius of the shell (i.e. $a \ll b$), the scattering peak and the scattering dip of the spectrum converge to the same frequency, giving rise to a Fano resonance [31]. The asymmetric core-shell structures can be studied using the modified multiple Mie scattering method [44–46]. However, it always involves complicated treatments of the all spherical harmonics, and is unlikely to give

#183368 - $15.00 USD Received 14 Jan 2013; revised 4 Mar 2013; accepted 4 Mar 2013; published 29 Mar 2013

closed-form expressions for the electric field, absorption and scattering cross-sections. In contrast, the TO approach allows us to derive all the physical quantities in closed forms. Therefore, it is more insightful when dealing with the 2D asymmetric core-shell structures.

The TO approach involves several steps. First, a logarithmic transformation maps the asymmetric DCMS (or MCDS) structure into a three-layer planar plasmonic system, which can be studied analytically, as depicted by Fig. 1(b). Note that similar conformal transformation was applied to study a pair of metal nanowires separated by a small gap [47]. Then, by expressing the electrostatic potential of the dipole source through a Fourier series, the SPP excitation associated with the transformed structure can be studied in the *k*-space. Finally, by applying an inverse Fourier transform to the *k*-space solution, the induced potential in the real space can be obtained

$$\phi^{\text{scatt}}(x,y)=\sum_{n=1}^{\infty}\frac{g\left(\alpha\eta_2^{2n}-\beta\right)}{\eta_1^{2n}\left(\eta_2^{2n}-\alpha\beta\right)}\begin{pmatrix}E_{0x}\cos\left(n\arg f(x,y)\right)\\+E_{0y}\sin\left(n\arg f(x,y)\right)\end{pmatrix}\left|f(x,y)\right|^{n} \tag{1}$$

where n is the angular momentum associated with the different scattering channels, and $f(x,y)$ is the function of the coordinate parameters (x, y)

$$f(x,y)=\ln\left[\frac{4d(x+iy)+\left(\sqrt{(b+d)^2-a^2}+\sqrt{(b-d)^2-a^2}\right)^2}{4d(x+iy)+\left(\sqrt{(b+d)^2-a^2}-\sqrt{(b-d)^2-a^2}\right)^2}\right]. \tag{2}$$

The constants g, η_1, η_2, α, and β are calculated as

$$g=\frac{\sqrt{(b+d)^2-a^2}\sqrt{(b-d)^2-a^2}}{d}, \tag{3}$$

$$\eta_1=\frac{\sqrt{(b+d)^2-a^2}+\sqrt{(b-d)^2-a^2}}{\sqrt{(b+d)^2-a^2}-\sqrt{(b-d)^2-a^2}}, \tag{4}$$

$$\eta_2=\frac{\sqrt{(b+a)^2-d^2}+\sqrt{(b-a)^2-d^2}}{\sqrt{(b+a)^2-d^2}-\sqrt{(b-a)^2-d^2}}, \tag{5}$$

$$\alpha=\frac{\varepsilon_1-1}{\varepsilon_1+1},\beta=\frac{\varepsilon_1-\varepsilon_2}{\varepsilon_1+\varepsilon_2}. \tag{6}$$

For DCMS structure $\varepsilon_1=\varepsilon_m$ and $\varepsilon_2=\varepsilon_d$, while for MCDS structure $\varepsilon_1=\varepsilon_d$ and $\varepsilon_2=\varepsilon_m$.

Considering the limit $x, y\to\infty$ in Eq. (1), the polarizability of the core-shell structure in the quasi-static limit can be calculated

$$\gamma=8\pi\varepsilon_0 g^2\xi \tag{7}$$

where

$$\xi=\sum_{n=1}^{\infty}\frac{n\left(\alpha\eta_2^{2n}-\beta\right)}{4\eta_1^{2n}\left(\eta_2^{2n}-\alpha\beta\right)}. \tag{8}$$

#183368 - $15.00 USD Received 14 Jan 2013; revised 4 Mar 2013; accepted 4 Mar 2013; published 29 Mar 2013

Note that the quasi-static solution is strictly valid only when the outer radius of the structure is smaller than about 10 nm. For cases that are beyond the quasi-static limit, the optical theorem can be used to model the radiative damping, important for larger sizes, as a fictive absorbing particle [48]. In the near-field approximation, the imaginary part of the Green's function has the form $\mathrm{Im}\left\{\overline{\overline{G}}(r,r_0)\right\} = -ik_0^2\overline{\overline{I}}/8\varepsilon_0$ [49] (where $\overline{\overline{I}}$ denotes the unity dyad), indicating that the induced electric field is uniform within the near-field:

$$\overline{E}^{\mathrm{sca}}\left(|\overline{r}| \ll \lambda\right) = -i\frac{k_0^2}{8\varepsilon_0}\gamma\overline{E}_0. \tag{9}$$

The modified polarizability of the core-shell structure can be calculated as

$$\gamma_m = \frac{\gamma}{1 - ik_0^2\gamma/8\varepsilon_0} = \frac{8\pi\varepsilon_0 g^2\xi}{1 - i\pi k_0^2 g^2\xi}. \tag{10}$$

Thus, we can obtain the extinction, scattering, and absorption cross-sections:

$$\sigma_{\mathrm{ext}} = k_0\,\mathrm{Im}\left\{\frac{\gamma_m}{\varepsilon_0}\right\} = 8\pi k_0 g^2\,\mathrm{Im}\left\{\frac{\xi}{1 - i\pi k_0^2 g^2\xi}\right\}, \tag{11}$$

$$\sigma_{\mathrm{sca}} = \left(\frac{k_0}{2}\right)^3\left|\frac{\gamma_m}{\varepsilon_0}\right|^2 = 8\pi^2 k_0^3 g^4\left|\frac{\xi}{1 - i\pi k_0^2 g^2\xi}\right|^2, \tag{12}$$

$$\sigma_{\mathrm{abs}} = \sigma_{\mathrm{ext}} - \sigma_{\mathrm{sca}} = 8\pi k_0 g^2\frac{\mathrm{Im}\{\xi\}}{\left|1 - i\pi k_0^2 g^2\xi\right|^2}. \tag{13}$$

We can see from Eq. (12) that the scattering peak occurs at a frequency that satisfies $\xi \to \infty$. For the scattering channel with an angular momentum *n*, this requires

$$\eta_2^{2n} = \alpha\beta. \tag{14}$$

Similarly, the reduced scattering corresponds to the scattering dip which happens at a frequency satisfying $\xi = 0$. For the *n*-th scattering channel, we have

$$\eta_1^2\left(\frac{\eta_2^{2n+2} - \alpha\beta}{\eta_2^{2n} - \alpha\beta}\right) = -\left(\frac{n+1}{n}\right)\left(\frac{\alpha\eta_2^{2n+2} - \beta}{\alpha\eta_2^{2n} - \beta}\right). \tag{15}$$

The condition given by Eq. (15) is also referred to as the cloaking condition [31]. It occurs when the negative polarizability of the plasmonic shell is properly tailored to suppress the electric dipole radiation from the inner particle. According to Eq. (15), the appearance of the scattering dip requires $\varepsilon_d > 1$.

3. Results and discussion

Figure 2 shows the scattering (solid line) and absorption (dashed line) cross-sections of a silver coated glass nanowire calculated using Eqs. (14) and (15). Here, the geometrical parameters are $a = 5$ nm , $b = 30$ nm . The left column corresponds to the numerical simulation results using finite element modeling (COMSOL Multiphysics) and the right column shows the analytical results based on transformation optics theory. We start by considering Fano resonances in the symmetric case, as shown in the top panels. The first Fano

#183368 - $15.00 USD Received 14 Jan 2013; revised 4 Mar 2013; accepted 4 Mar 2013; published 29 Mar 2013

resonance mode is excited at 340 nm, where a scattering dip associated with an absorption peak appears in the spectrum. This can be explained by Eq. (14) and Eq. (15). The interference of the dark scattering state [described by Eq. (15)] with the dipolar mode of the shell [described by Eq. (14)] enables a Fano resonance. In other words, the scattering peak and the scattering dip must converge to the same frequency, requiring that $b \gg a$. For a symmetric core-shell structure ($d = 0$), the left side of Eq. (14) is reduced to $(b/a)^{2n}$. As $b \gg a$, all the SPP resonances degenerates at the frequency where $\varepsilon_m = -\varepsilon_d$. In this case, only the dipolar resonance (with angular momentum $n = 1$) can be excited.

From Eqs. (14) and (15), we can see that increasing the displacement d will in turn increase the number of resonance modes supported by the structure, thereby inducing higher-order Fano resonances. This can also be observed in Fig. 2. In the middle panels, a displacement of 20 nm is introduced to the glass core. The first-order Fano resonance is red-shifted with respect to the symmetric case and has the reduced modulation depth, while the second-order resonance occurs at 339 nm, close to the Fano resonance of the symmetric structure. The increase of the geometric asymmetry corresponds to further increase of the interaction between the inner and outer boundaries of metal, thereby inducing additional higher-order Fano resonances [47]. As shown in the bottom panels where the core offset $d = 24$ nm, three distinct Fano dips with asymmetric profiles appear in the scattering spectrum, and the first Fano mode shifts to wavelength 430 nm. In the extreme case with $d = b - a$ (corresponding to an asymmetric core-shell structure with a geometric singularity at the touching point [3, 50]), the left side of Eq. (14) is reduced to 1, indicating that the structure shows a broadband response to the incident light. Here, we highlight that the two interfering modes associated with each Fano resonance results from the same scattering states, namely, the dipole state and the anti-bonding cloaking state. Because this cloaking state is an anti-resonant feature, this Fano resonance is independent of the direction of the incident electric field, and may be detected at any observation angle. This is a major difference from conventional plasmonic Fano resonances, which is often strongly polarization dependent.

In order to gain further physical insights into the multiple Fano resonances arising from the symmetry breaking, we study the near-field property of the asymmetric core-shell structures. Figure 3 displays the electric field profiles at each absorption peak and the corresponding scattering peak. The structure considered here is same as the one studied in the bottom panels of Fig. 2 ($R_i = 5$ nm, $R_o = 30$ nm, $d = 24$ nm). As we can see from the calculated results, at the wavelengths of the scattering peaks (top row, Fig. 3), the surface plasmon field is spread out over the outer surface of core-shell structure, giving rise to a large scattering efficiency. On the contrary, at the absorption peaks (bottom row, Fig. 3), the plasmon field is mostly confined around the dielectric core, leading to a smaller scattering efficiency.

#183368 - $15.00 USD Received 14 Jan 2013; revised 4 Mar 2013; accepted 4 Mar 2013; published 29 Mar 2013

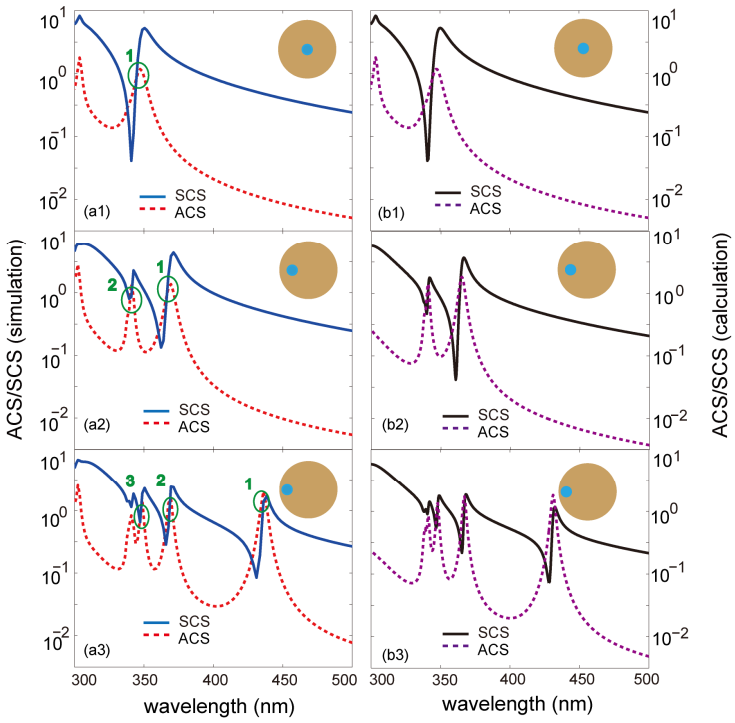

Fig. 2. The scattering (solid line) and absorption (dashed line) cross sections for glass nanowires (the radius $a = 5\ nm$) with concentric [(a1), (b1) $d = 0\ nm$] and non-concentric [(a2), (b2) $d = 20\ nm$ and (a3), (b3) $d = 24\ nm$] silver shells (the radius $b = 30\ nm$). The left column corresponds to the simulation results and the right corresponds to the analytical solutions.

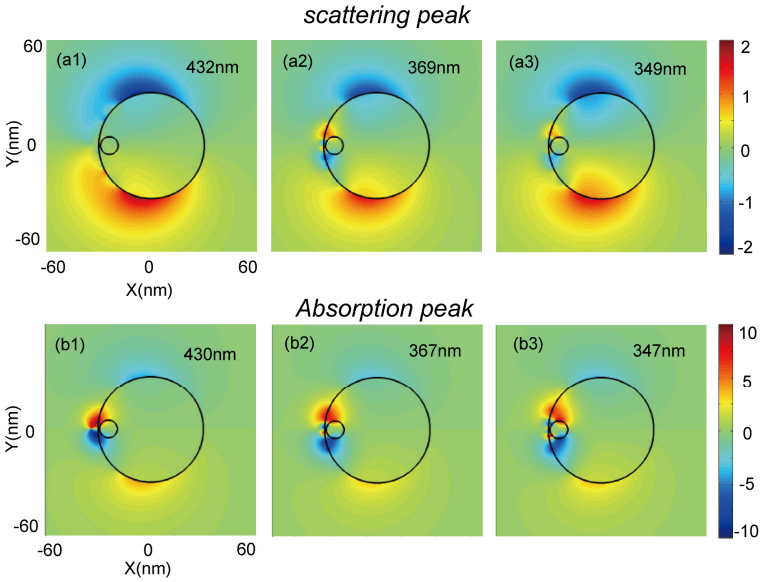

Fig. 3. Snapshots of the electric field distributions for a nonconcentric glass-core silver-shell nanowires ($a = 5\ nm$, $b = 30\ nm$, $d = 24\ nm$) at the scattering and the absorption peak wavelengths (c.f. Figure 2 (a3)).

#183368 - $15.00 USD Received 14 Jan 2013; revised 4 Mar 2013; accepted 4 Mar 2013; published 29 Mar 2013

To understand how the core offset d affect the Fano resonance behaviour, a plot of the normalized scattering cross section versus the core offset d and the wavelength for the above structure ($a = 5\ nm$, $b = 30\ nm$) is shown in Fig. 4. We can clearly see that the increase of d gives rise to the increasing number of resonance modes, while their intensities decrease. Since there is a trade-off between the number of resonance modes and the modulation depth, only the appropriately designed structure provides the optimized multiple Fano-resonance features. In our case, the structures with a core offset ranging from 20 nm to 24 nm offers multiple Fano profiles with acceptable modulation depth.

The impact of dielectric constant of the core on the resonance profile is shown in Fig. 5, where the scattering and absorption cross sections are plotted for the dielectric-core silver-shell structures with increasing core offsets (d = 0 nm, d = 20 nm, and d = 24 nm). As the refractive index of the inner core increases, all the resonance modes shift to lower frequencies. This result demonstrates the possibility of engineering the resonance spectrum of the structure by changing the material of the inner core.

One distinct property of the Fano resonance is the narrow line-width which is advantageous for sensing applications. By changing the refractive index of the surroundings, one can induce a pronounced shift of the resonance which can be observed by monitoring the transmittance at a wavelength close to it. Higher-order Fano resonances enable the multi-wavelength sensing as the Fano resonance can be modified at several spectral positions simultaneously. Here, to evaluate the sensing performance of our structure, we calculate the figure of merit, which is defined as the resonance wavelength shift upon the change of the refractive index of the surrounding medium n, divided by the resonance width: $FoM = \dfrac{\partial \lambda}{\partial n \Delta \lambda}$. Figure 6 shows the FOM for the glass nanowire with silver coating ($a = 5\ nm$, $b = 30\ nm$), as a parametric dependence on the geometric asymmetry, which modifies the resonance wavelength. We can observe the increase of FoM with the increase of the geometric asymmetry resulting also in shift of the resonance wavelength.

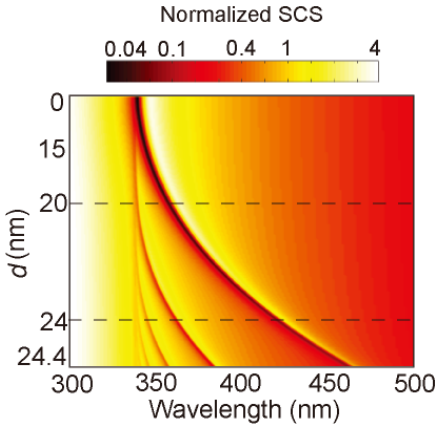

Fig. 4. Plot of the scattering cross section normalized to the diameter versus the core offset d and the wavelength for a glass nanowire with asymmetric silver coating ($a = 5\ nm$, $b = 30\ nm$).

#183368 - $15.00 USD Received 14 Jan 2013; revised 4 Mar 2013; accepted 4 Mar 2013; published 29 Mar 2013

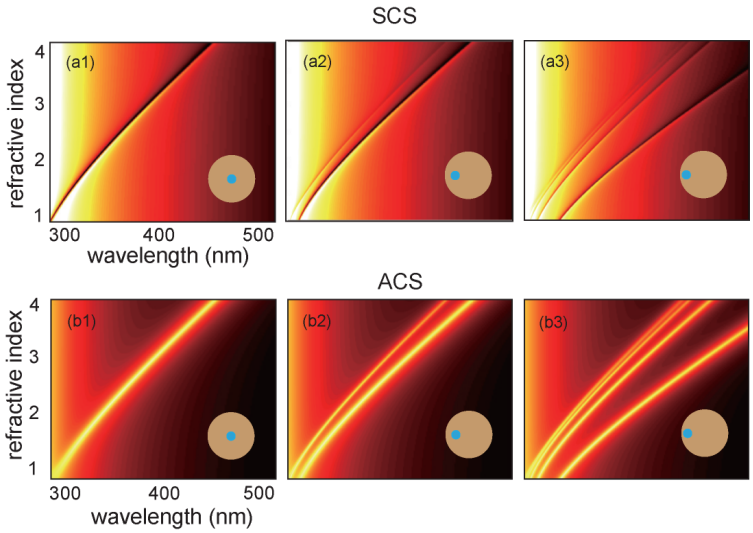

Fig. 5. Parametric plots of scattering cross sections and absorption cross sections versus the refractive index of the dielectric core and the wavelength for a dielectric nanowire with asymmetric silver coating ($a = 5\ nm$, $b = 30\ nm$). In left panels, $d = 0\ nm$; In middle panels, $d = 20\ nm$; In right panels, $d = 24\ nm$.

We now move on to studies of the metallic core with dielectric shell configuration. Similar to the DCMS case, this structure shows that multiple Fano resonances appear as the coating become asymmetric, except that the mode shows a blue shift with the increased asymmetry—the opposite trend than for DCMS structures. Another difference worth noting is that, in the DCMS case, all the plasmonic resonances have symmetric field profiles and are excited below the surface plasmon frequency, where $\varepsilon_{metal} < -\varepsilon_{dielectric}$. In other words, the resonances are distributed in a broad frequency range. |In contrast, for the MCDS structure, the resonances are all asymmetric modes, thus can only be excited in the a relatively narrow frequency range where $-\varepsilon_{dielectric} < \varepsilon_{metal} < -1$. The extension of bandwidth can be achieved through increasing the permittivity of the dielectric core. This provides additional degree of freedom for tailoring the Fano resonance spectrum. Finally, by comparing Fig. 7 and Fig. 2, we find that the MCDS structures provide higher modulation depth than the DCMS ones. This is because for the MCDS configuration the dark modes are confined around the core and, as a result, suffer from higher Ohmic losses.

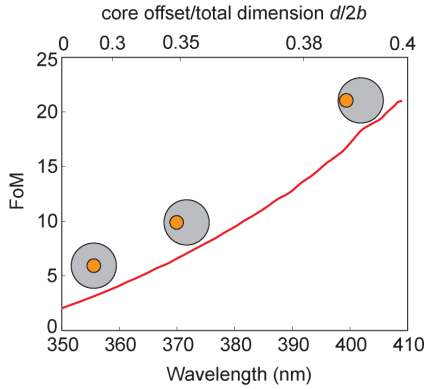

Fig. 6. The dependence of the FoM on the asymmetry of the sensing structure consisting of the glass nanowire with silver coating ($a = 5\ nm$, $b = 30\ nm$) for first-order Fano resonance.

#183368 - $15.00 USD Received 14 Jan 2013; revised 4 Mar 2013; accepted 4 Mar 2013; published 29 Mar 2013

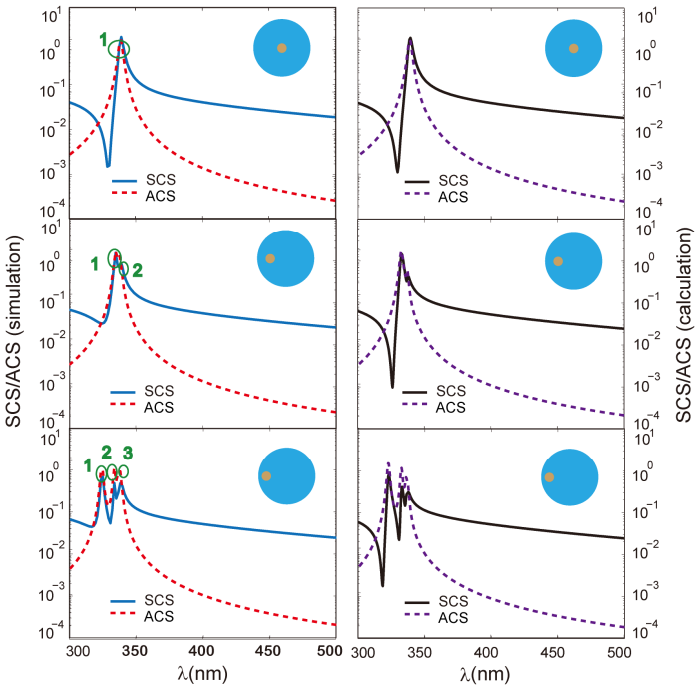

Fig. 7. The scattering (solid line) and absorption (dashed line) cross sections for silver nanowires (the radius $a = 5\ nm$) with concentric [(a1), (b1) $d = 0\ nm$] and non-concentric [(a2), (b2) $d = 20\ nm$ and (a3), (b3) $d = 24\ nm$] glass shells (the radius $b = 30\ nm$). The left column corresponds to the simulation results and the right one corresponds to the analytical solutions.

Conclusion

We have shown that multiple Fano-like resonances can be realized with nonconcentric single layer core-shell nanostructures. By appropriately tuning the core offset and choosing the materials, multiple Fano resonances can be observed with prominent modulation depth. Compared to previous approaches for achieving multiple Fano resonances where multiple elements are always involved, our design is easier to realize in practice. The design can be extended to three-dimensional case. As has been experimentally observed in silica-gold core-shell nanoparticles, the core offset allows for the emergence of high-order modes [37]. Therefore, by appropriately tuning the geometrical parameters, multiple Fano resonances are expected to occur in spherical nano-shells. We envision fabrication of these core-shell nanostructures with current nanofabrication techniques and their applications in multifrequency biosensing and signal processing.

Acknowledgments

This work is supported by the Royal Society Newton International Fellowship and EPSRC (UK).

#183368 - $15.00 USD Received 14 Jan 2013; revised 4 Mar 2013; accepted 4 Mar 2013; published 29 Mar 2013